AD-A193 022 FIELD-ALIGNED STRUCTURE OF THE STORM TIME PC 5 WAVE OF 1/1
NOVEMBER 14-15 197.. (U) AEROSPACE CORP EL SEGUNDO CA
SPACE SCIENCES LAB K TAKAHASHI ET AL. 01 FEB 88
UNCLASSIFIED TR-0086A(2940-05)-3 SD-TR-88-05 F/G 4/1 NL

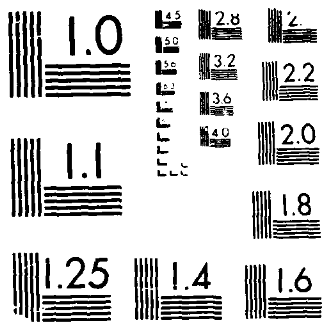

MICROCOPY RESOLUTION TEST CHART

REPORT SD-TR-88-05

Field-Aligned Structure of the Storm Time Pc 5 Wave of November 14-15, 1979

K. TAKAHASHI and P. R. HIGBIE
Los Alamos National Laboratory
Los Alamos, NM 87545

J. F. FENNELL
Space Sciences Laboratory
Laboratory Operations
The Aerospace Corporation
El Segundo, CA 90245

and

E. AMATA
Instituto di Fisica dello Spazio Interplanetario
Rome, Italy

1 February 1988

Prepared for

SPACE DIVISION
AIR FORCE SYSTEMS COMMAND
Los Angeles Air Force Base
P.O. Box 92960, Worldway Postal Center
Los Angeles, CA 90009-2960

This report was submitted by The Aerospace Corporation, El Segundo, CA 90245, under Contract No. F04701-85-C-0086-P00016 with the Space Division, P.O. Box 92960, Worldway Postal Center, Los Angeles, CA 90009-2960. It was reviewed and approved for The Aerospace Corporation by H. R. Rugge, Director, Space Sciences Laboratory.

Lt Clarence V. Wilcox/CLTPC was the project officer for the Mission-Oriented Investigation and Experimentation (MOIE) Program.

This report has been reviewed by the Public Affairs Office (PAS) and is releasable to the National Technical Information Service (NTIS). At NTIS, it will be available to the general public, including foreign nationals.

This technical report has been reviewed and is approved for publication. Publication of this report does not constitute Air Force approval of the report's findings or conclusions. It is published only for the exchange and stimulation of ideas.

Clarence V Wilcox

CLARENCE V. WILCOX, Lt, USAF
MOIE Project Officer
SD/CLTPC

Raymond M Leong

RAYMOND M. LEONG, Major, USAF
Deputy Director, AFSTC West Coast Office
AFSTC/WCO OL-AB

UNCLASSIFIED

SECURITY CLASSIFICATION OF THIS PAGE

REPORT DOCUMENTATION PAGE

1a. REPORT SECURITY CLASSIFICATION Unclassified	1b. RESTRICTIVE MARKINGS
2a. SECURITY CLASSIFICATION AUTHORITY	3. DISTRIBUTION / AVAILABILITY OF REPORT Approved for public release; distribution unlimited.
2b. DECLASSIFICATION / DOWNGRADING SCHEDULE	
4. PERFORMING ORGANIZATION REPORT NUMBER(S) TR-0086A(2940-05)-3	5. MONITORING ORGANIZATION REPORT NUMBER(S) SD-TR-88-05
6a. NAME OF PERFORMING ORGANIZATION The Aerospace Corporation Laboratory Operations 6b. OFFICE SYMBOL (If applicable)	7a. NAME OF MONITORING ORGANIZATION Space Division
6c. ADDRESS (City, State, and ZIP Code) El Segundo, CA 90245	7b. ADDRESS (City, State, and ZIP Code) Los Angeles Air Force Base Los Angeles, CA 90009-2960
8a. NAME OF FUNDING / SPONSORING ORGANIZATION 8b. OFFICE SYMBOL (If applicable)	9. PROCUREMENT INSTRUMENT IDENTIFICATION NUMBER F04701-85-C-0086-P00016
8c. ADDRESS (City, State, and ZIP Code)	10. SOURCE OF FUNDING NUMBERS PROGRAM ELEMENT NO. / PROJECT NO. / TASK NO. / WORK UNIT ACCESSION NO.

11. TITLE (Include Security Classification)
Field-Aligned Structure of the Storm Time Pc 5 Wave of November 14-15, 1979

12. PERSONAL AUTHOR(S)
Takahashi, K., and Higbie, P. R., *Los Alamos National Laboratory*,; Fennell, Joseph F.,

13a. TYPE OF REPORT	13b. TIME COVERED	14. DATE OF REPORT (Year, Month, Day)	15. PAGE COUNT
	FROM ____ TO ____	1 February 1988	39

16. SUPPLEMENTARY NOTATION

17. COSATI CODES			18. SUBJECT TERMS (Continue on reverse if necessary and identify by block number)
FIELD	GROUP	SUB-GROUP	Magnetic Pulsations, Storms, Magnetosphere, Waves

19. ABSTRACT (Continue on reverse if necessary and identify by block number)

Magnetic field data from the four satellites--SCATHA (P78-2), GOES 2, GOES 3, and GEOS 2--have been analyzed to examine the magnetic-field-aligned structure of a storm time Pc 5 wave which occurred on November 14-15, 1979. The wave had both transverse and compressional components. At a given instance, the compressional and the radial components oscillated in phase or 180° out of phase, and the compressional and the azimuthal components oscillated +90° or -90° out of phase. In addition, each component changed its amplitude with magnetic latitude: the compressional component had a minimum at the magnetic equator, whereas the transverse components had a maximum at the equator and minima several degrees off the equator. At 180° relative phase switching among the components occurred across the latitudes of amplitude minima. From these observations, the field-line displacement of the wave is confirmed to have an antisymmetric standing structure about the magnetic equator with a parallel wave length of a few earth radii. We also observed other intriguing properties of the wave, such as different parallel wavelengths of different field components and small-amplitude second harmonics near the nodes. A dielectric tensor appropriate for the ring

20. DISTRIBUTION / AVAILABILITY OF ABSTRACT ☐ UNCLASSIFIED/UNLIMITED ☒ SAME AS RPT. ☐ DTIC USERS	21. ABSTRACT SECURITY CLASSIFICATION Unclassified
22a. NAME OF RESPONSIBLE INDIVIDUAL	22b. TELEPHONE (Include Area Code) / 22c. OFFICE SYMBOL

DD FORM 1473, 84 MAR

83 APR edition may be used until exhausted.
All other editions are obsolete.

SECURITY CLASSIFICATION OF THIS PAGE

UNCLASSIFIED

UNCLASSIFIED

SECURITY CLASSIFICATION OF THIS PAGE

12. PERSONAL AUTHOR(S) (Continued)

The Aerospace Corporation; and Amata, E., Instituto di Fisica dello Spazio Interplanetario.

19. ABSTRACT (Continued)

current plasma is found to give an explanation for the relation between the polarization and the propagation of the wave. However, plasma data available from SCATHA do not support either the drift-mirror instability of Hasegawa or the coupling between a drift-mirror wave and a shear Alfvén wave, as discussed by Walker and coworkers.

UNCLASSIFIED

SECURITY CLASSIFICATION OF THIS PAGE

PREFACE

The authors are grateful to L. Chen, A. Hasegawa, and C. S. Lin for useful comments, and to B. Wilken for providing an edited version of GEOS 2 magnetic field data. The magnetic field data of GOES 2 and GOES 3 were supplied by National Geophysical Data Center, Boulder, Colorado.

CONTENTS

FIGURES

1. Introduction

Storm time Pc 5 waves (period = 150-600 s), which perhaps are the lowest-frequency and largest-amplitude among storm time ULF waves, were recognized in the late 60's and have since been the subject of many observational as well as theoretical studies. Early work on this subject can be found in Brown et al. [1968], Sonnerup et al.[1969], Hasegawa [1969], and Lanzerotti et al. [1969].

Recent observations with multiple satellites and ground-based radar established the variation of the amplitude and phase of storm time Pc 5 waves across the ambient magnetic field. The waves are observed to propagate westward with respect to the ground [Walker et al., 1982; Allan et al., 1982] and geostationary satellites [Takahashi et al., 1985a; Lin and Barfield, 1985]. The waves have a large azimuthal wave number ($|m|$ = 20-100), and their typical propagation velocity and azimuthal wavelength are 5-50 km/s and 1000-10000 km, respectively. For one case, the radial extent of the wave was observed to be as large as 1.7 R_E [Takahashi et al.,1985b]. The oscillation phase of the wave field with radial distance (or with latitude for ground-based observations) is nearly constant [Walker et al., 1982; Takahashi et al., 1985a] or varies much slower than for Pc 5 waves that are externally driven field-line resonance [Allan et al., 1982].

In spite of its importance in theoretically discussing the mechanism for wave excitation [e.g., Southwood, 1976], the field-aligned structure of storm time Pc 5 waves is much less understood than the azimuthal or radial structure. It is usually assumed that the waves have a standing (rather than propagating) structure along the field line, and there is some evidence to support this assumption in the form of the quadrature phase relation between the mutually orthogonal electric and magnetic field components [Walker et al., 1983; Pokhotelov et al., 1985]. The standing structure of the wave has been usually inferred from observations such as the phase and amplitude relation among the components of the electric and magnetic fields of the wave [Walker et al., 1983; Pokhotelov et al., 1985] or particle flux modulation caused by the wave [Takahashi and Higbie, 1986]. Only rare observations of the nodal structure of storm time Pc 5 waves have been made with spacecraft with varying magnetic latitude [Takahashi et al., 1985b]. Regarding the wavelength along the field line, Nagano and Araki [1983] argued that the waves have a significant amplitude only near the equator. Their argument was based on a statistical study of the magnetic field data from GOES 3 (magnetic latitude = 5°) and GOES 3 (9°). Probably owing to insufficient spatial coverage of the data, these studies led to various standing wave models for storm time Pc 5: a symmetric wave [Walker et al., 1982], an antisymmetric wave [Pokhotelov et al., 1985; Takahashi and Higbie, 1986], and a combination of a symmetric wave and an antisymmetric wave [Walker et al., 1983; Takahashi et al., 1985b].

Hereinafter we define the symmetry of a standing wave in terms of field line displacement. With this definition, fixed-end, odd-mode (even-mode) standing waves, which have an antinode (node) of field-line displacement at the equator, are symmetric (antisymmetric). Since the transverse component of the perturbed magnetic field is proportional to the tilt of the local field line, a symmetric (antisymmetric) wave has a node (antinode) at the equator for the transverse component. In contrast, since magnetic field compression is inversely proportional to the distance between field lines (for one-dimensional compression), a symmetric (antisymmetric) wave has an antinode (node) at the equator for the compressional component.

In this report, we study the field-aligned structure of a storm time Pc 5 wave using magnetic field data from the four satellites—SCATHA, GOES 2, GOES 3, and GEOS 2 —which were located at or near geostationary orbit. We have chosen a Pc 5 wave which occurred on November 14-15, 1979, because the event lasted for longer than 50 hours, and because from previous reports on the same event [Higbie et al., 1982; Takahashi et al., 1985a], we have some knowledge on the propagation characteristics and local time extent of the wave.

In support of a previous study based on energetic particle data [Takahashi and Higbie, 1986], we obtain clear evidence that the wave had an antisymmetric standing structure along the ambient magnetic field line. Furthermore, we demonstrate that the wave length parallel to the field line was only a few earth radii, which is much shorter than the length of the field line itself. These observations should make a considerable impact to the theory of storm time Pc 5 waves. The organization of this report is as follows. In section 2, experiments and data are described. In Section 3, the data are analyzed. In Section 4, a phenomenological model of a standing wave is presented. In Section 5, we discuss the result of the data analysis in relation to the theories of the propagation and generation of hydromagnetic waves. Section 6 is the conclusion.

2. Experiments and Data

The magnetic field data have been acquired with fluxgate magnetometers. The descriptions of the experiments have been given by Fennell [1982] for SCATHA, by Grubb [1975] for GOES 2 and GOES 3, and by Knott [1982] for GEOS 2. We used 1-min vector magnetic field data, which were obtained by taking running averages of the original high-time-resolution data. We also used data from the plasma experiment on board SCATHA [Fennell, 1982] to determine ion pressure.

We were very fortunate that the four satellites were located at various magnetic latitudes. The geostationary satellites GOES 2, GOES 3, and GEOS 2 were located on the geographic equator at the geographic longitudes of 107°W, 135°W, and 15°E, which correspond to the magnetic latitudes of $\sim 9^\circ$N, $\sim 5^\circ$N, and $\sim 1^\circ$N, if we assume a centered dipole with its north pole directed to 78.3°N and 291.0°E in geographic coordinates. SCATHA had an elliptical orbit with an orbital period of 23.6 hours. The apogee and perigee were 7.8 R_E and 5.3 R_E, respectively, and the inclination of the orbit was 7.8°. During the course of the November 14-15 event, its magnetic latitude varied between -7° and 0°.

3. Data Analysis

Figure 1 summarizes the Pc 5 activity associated with the geomagnetic storm of November 13-15, 1979. At the top is the hourly D_{st} index, and at the bottom is the local time of the satellites, both plotted as a function of universal time. In the lower panel, the presence of a Pc 5 wave as observed by each spacecraft is indicated by the heavy portion of the orbit traces. The wave lasted at least the 54-hour period between 1800UT of November 13 and 2400UT of November 15. This corresponds to the recovery phase of the geomagnetic storm shown in the upper panel. From 0700UT of November 14 to 0500UT of November 15, the wave was observed over the entire dayside; therefore it deserves the designation of "a global Pc 5 wave" [Higbie et al., 1982]. We chose this 22-hour interval for a detailed study of the spatial structure of the wave.

3.1 Latitudinal variation of phase and amplitude

In Figure 2 we show the SCATHA magnetic field data to demonstrate the continuous wave activity. At the top are the 1-min averages of the magnetic field components B_V, B_D, and B_H, where $\hat{e}_H$ (northward) is

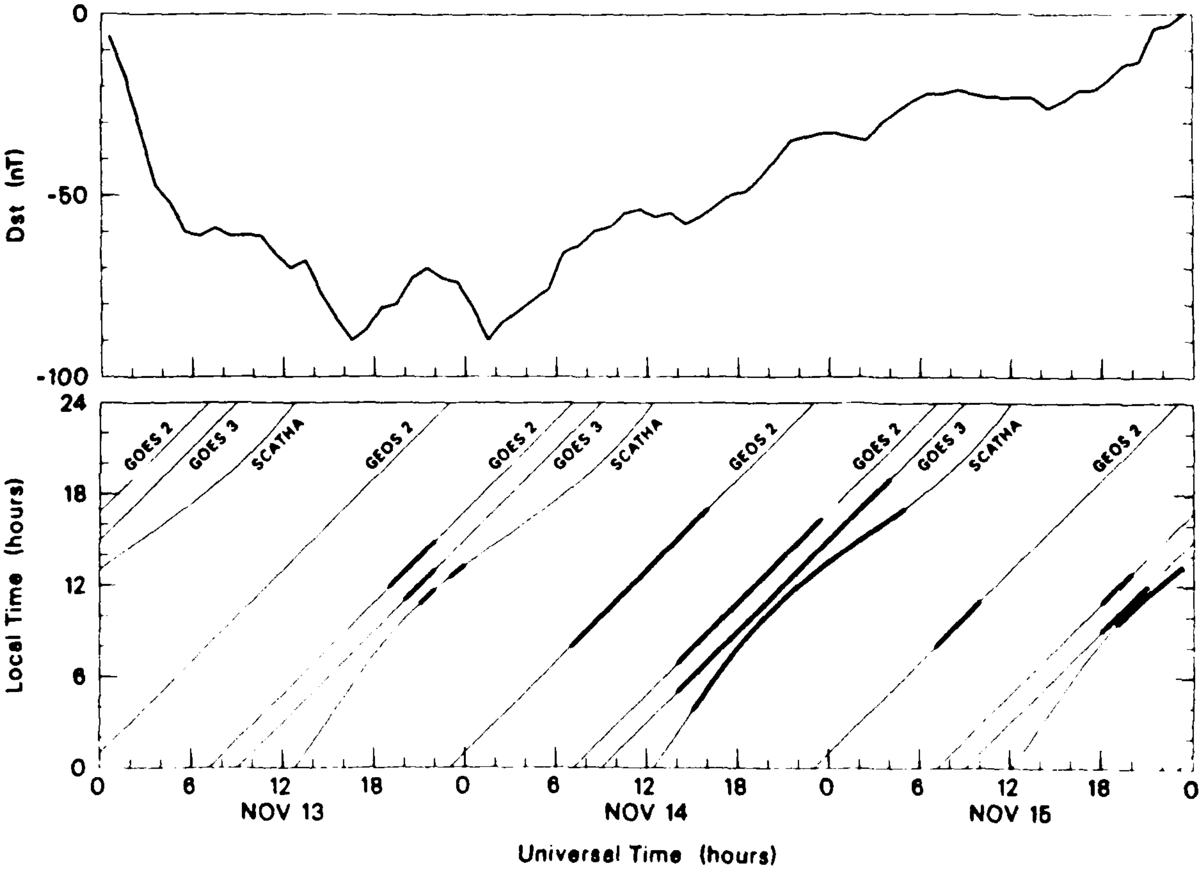

Figure 1. Overall Illustration of Pc 5 Activity (lower panel) and Its Relation to the Ring Current Intensity (upper panel) During the Interval of 13-15 November 1979. In the lower panel, the local time of the four satellites is illustrated as a function of universal time. The heavy portion of the orbit trace means the presence of a Pc 5 wave.

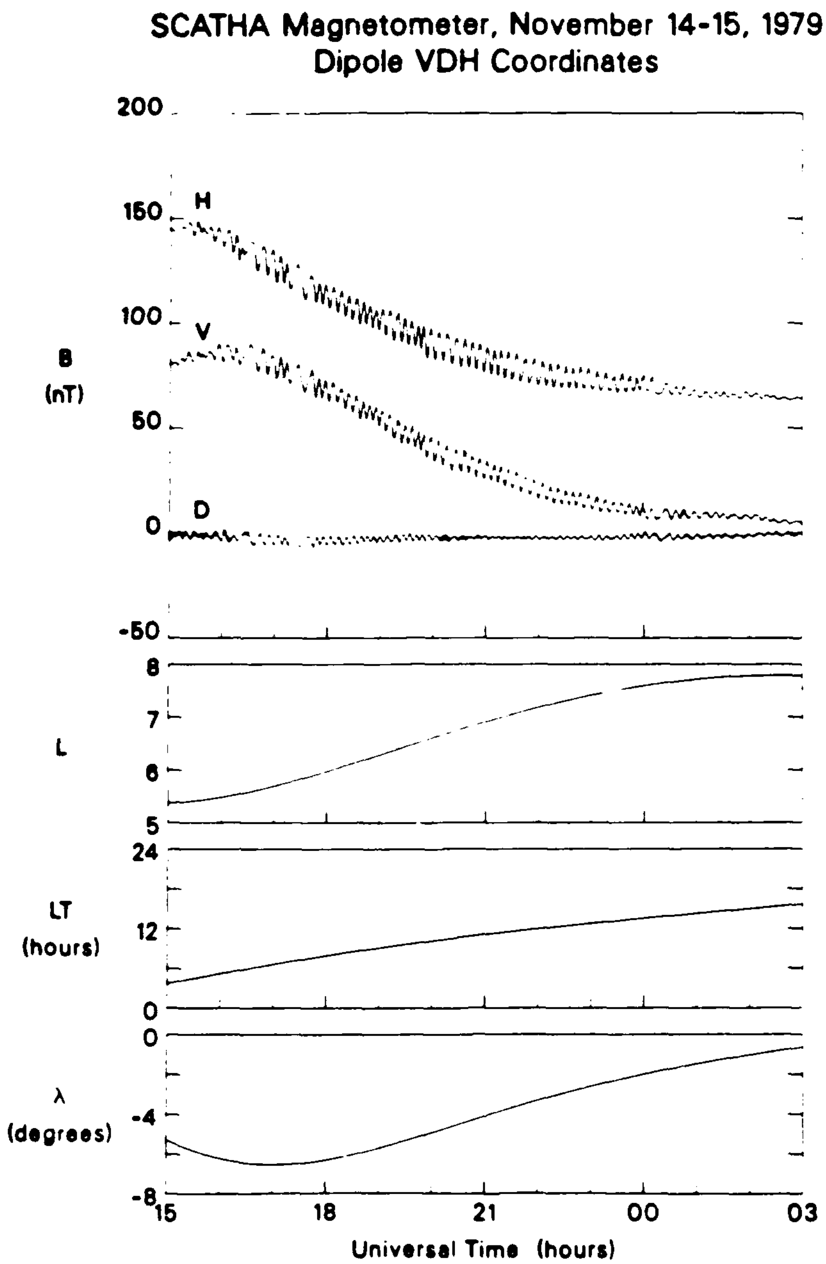

Figure 2. SCATHA Magnetic Field Showing a Continuous Wave Activity for the 12-hr Period (upper panel). The lower three panels show the position of the satellite in terms of magnetic shell parameter (L), local time (LT), and magnetic latitude (λ).

antiparallel to the geomagnetic dipole, $\hat{e}_D$ (eastward) is in the direction of $\hat{e}_H \times \underline{R}_s$, where $\underline{R}_s$ is the radial vector of the satellite with respect to the center of the earth, and $\hat{e}_V$ (outward)= $\hat{e}_D \times \hat{e}_H$ completes a triad. At the bottom are the L value, local time, and the magnetic latitude (λ) of the satellite. We used the centered dipole mentioned above to calculate L and λ.

The wave is present continuously for the 12-hour interval shown. It has an average period of 600 s, and all the three components show an oscillation of the same periodicity. The H component, which has the largest amplitude overall, demonstrates the highly compressional nature of the oscillation. The background field changes smoothly with the combined effects of the varying L and λ.

For the interval of 1900-2300UT, we obtained $\beta_{\parallel}$ = 0.16-0.21 and $\beta_{\perp}$ = 0.23-0.30 from the SCATHA ion data (17 eV to 300 keV), where β is the ratio of plasma pressure to magnetic field pressure, and the subscripts "$\parallel$" and "$\perp$" refer to the components parallel and perpendicular to the ambient magnetic field. These values do not satisfy Hasegawa's [1969] condition for drift-mirror instability

$$1 + \beta_{\perp}\left(1 - \frac{\beta_{\perp}}{\beta_{\parallel}}\right) < 0.$$

The same interval is shown in Figure 3 using an expanded time

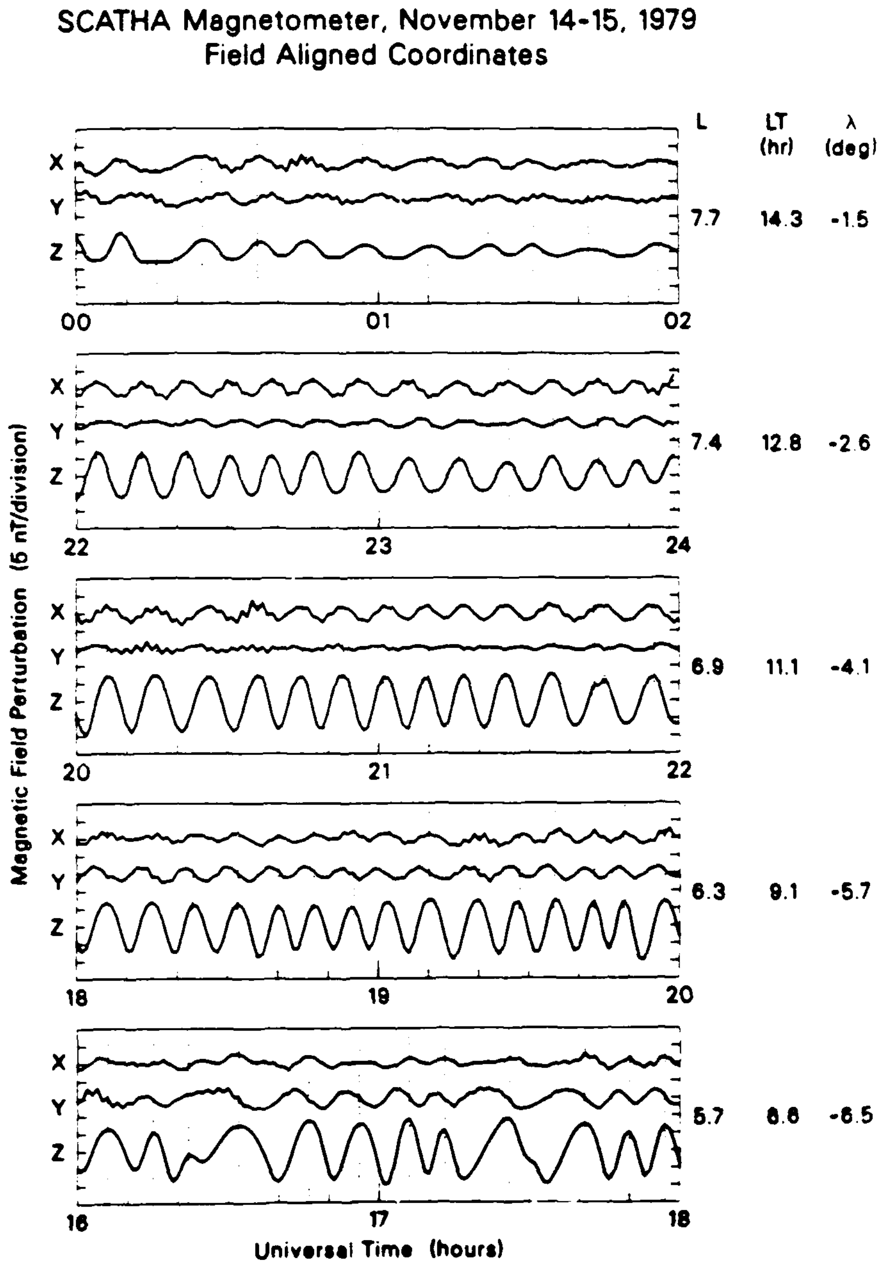

Figure 3. Sequence of SCATHA Magnetic Field Data Presented in the Detrended Field-Aligned Coordinates. The position parameters given at the right of each panel correspond to the center of the 2-hr segment. Vertical dotted lines are drawn to indicate the maxima of b_z.

scale and a field-aligned coordinate system. In this system, $\hat{e}_z$ (northward) is along the ambient field averaged over a 1-hour interval about each 1-min data point, $\hat{e}_y$ (eastward) is parallel to $\hat{e}_z \times \underline{R}_s$, and $\hat{e}_x$ (outward) = $\hat{e}_y \times \hat{e}_z$ completes the triad. For the z component, the trend has been removed by running average. In the text, the perturbation in the field components shall be denoted as b_x, b_y, or b_z hereinafter. We have organized the five 2-hour segments according to the geomagnetic latitude of the satellite, so the time runs from bottom to top. The L value, local time, and λ are given for the center of each 2-hour segment. In Figure 4 we have added the magnetic field data from the three geostationary satellites located at fixed magnetic latitudes. The format is the same as in Figure 3. All the data were taken around noon.

The key features to be noticed in Figure 3 and Figure 4 are the *phase and amplitude relations among the field components*. For example, b_y leads b_x by 90° at $\lambda = -6.5^\circ$ and -5.7°, b_y has a small amplitude at $\lambda = -4.1^\circ$ so that the relative phase cannot be defined, and at $\lambda = -2.6^\circ$ and 1.2°, b_x leads b_y by 90°. At $\lambda = 4.7^\circ$, b_y again has a very small amplitude. At $\lambda = 9.2^\circ$, b_x has a small amplitude, making it difficult to establish the phase lag. Amplitude and phase variations are also observed for b_z.

Although the wave event lasted very long, it is still possible that the amplitude changed with universal time, local time, or L value, as well as with magnetic latitude. Thus, use of raw amplitude makes the modeling of the field-aligned structure somewhat difficult. For this

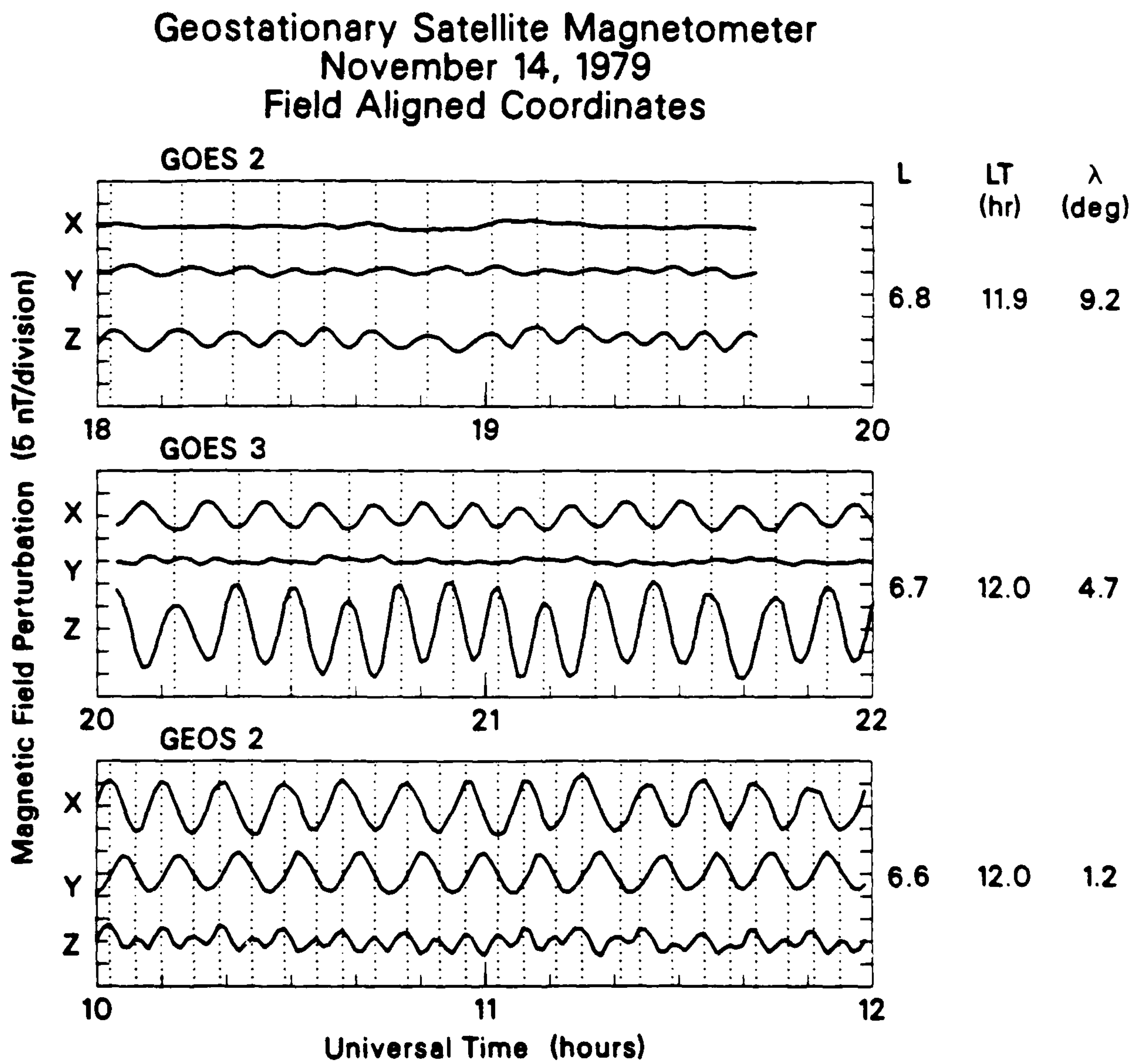

Figure 4. Same as Figure 3, Except for the Satellites

reason we introduced a normalized amplitude

$$\hat{b}_\alpha \equiv \left(\frac{\langle b_\alpha^2 \rangle}{\langle b_x^2 \rangle + \langle b_y^2 \rangle + \langle b_z^2 \rangle} \right)^{1/2}$$

to describe the variation of relative amplitudes among the field components with magnetic latitude. Here α = x, y, or z, and $\langle b_\alpha^2 \rangle$ is the mean-square amplitude of the magnetic field component obtained by integrating its power spectral density over the frequency range occupied by the wave. The spectral analysis was done on each of the 2-hour segments shown in Figures 3 and 4. In the same spectral analysis, the relative phases among the magnetic field components were also obtained. We denote by $\phi_{\alpha\beta}$ the relative phase of component α with respect to component β.

The normalized amplitude and the relative phase are illustrated in Figure 5 and Figure 6, respectively, as a function of magnetic latitude. The circles are the observational data points, and the curves are given by a model standing wave described below. In Figure 5, it is clear that the transverse components have a maximum amplitude near the magnetic equator and a minimum several degrees off the equator. In contrast, the compressional component has a minimum amplitude near the equator. In Figure 6, it is seen that the relative phase ϕ_{xy} or ϕ_{yz} is either -90° or 90°, and a switching occurs somewhere between $\lambda = -5^\circ$ and -3°. The relative phase ϕ_{zx} is either 0° or 180°, and a switching occurs somewhere between λ =

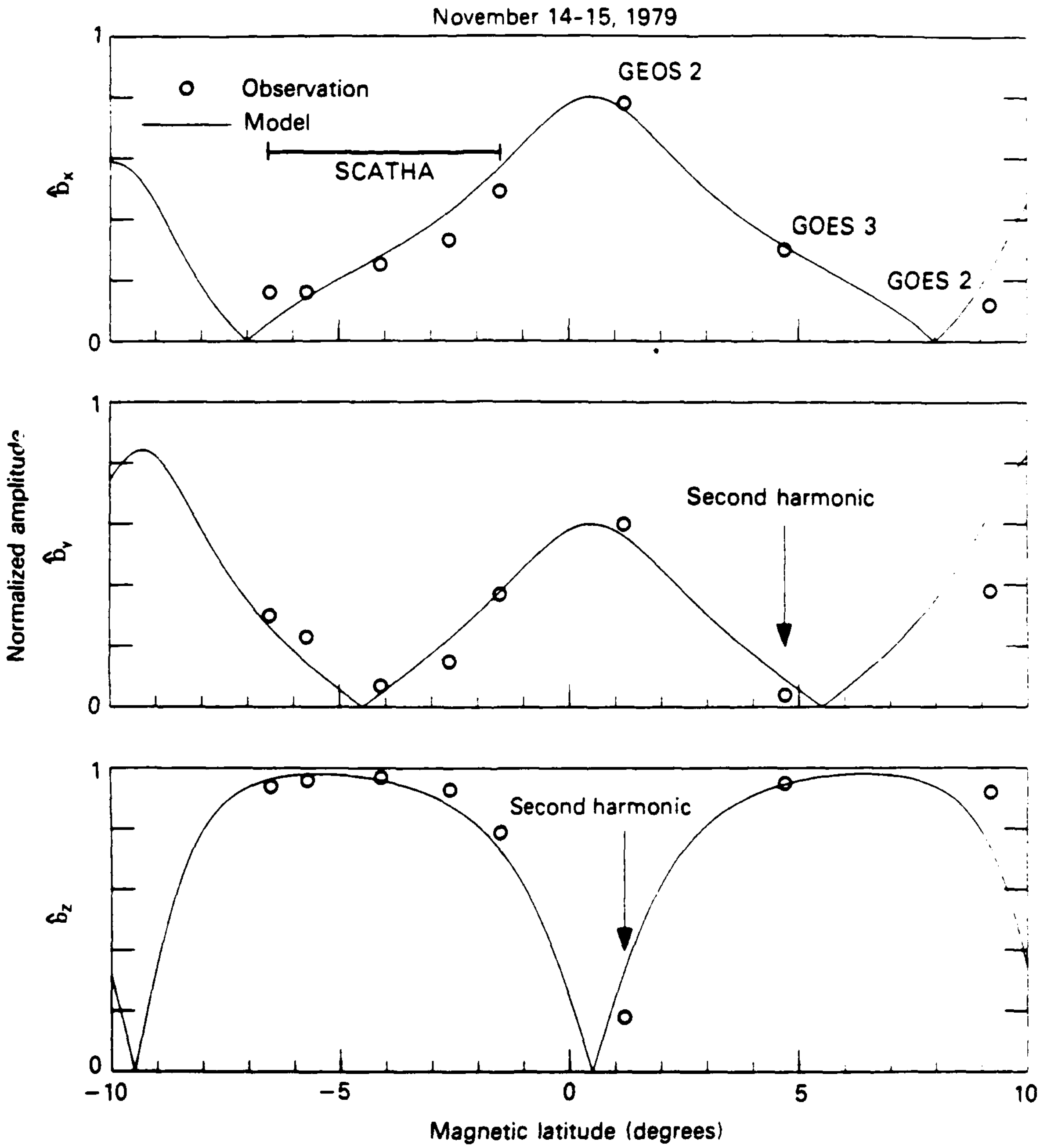

Figure 5. Normalized Amplitude of the Wave as a Function of Magnetic Latitude Given from Observation (circles) and a Model (curves). Spacecraft associated for the data points are indicated in the top panel. The arrows indicate the latitudes where a harmonic was observed. See text for the definition of the normalized amplitude and the model.

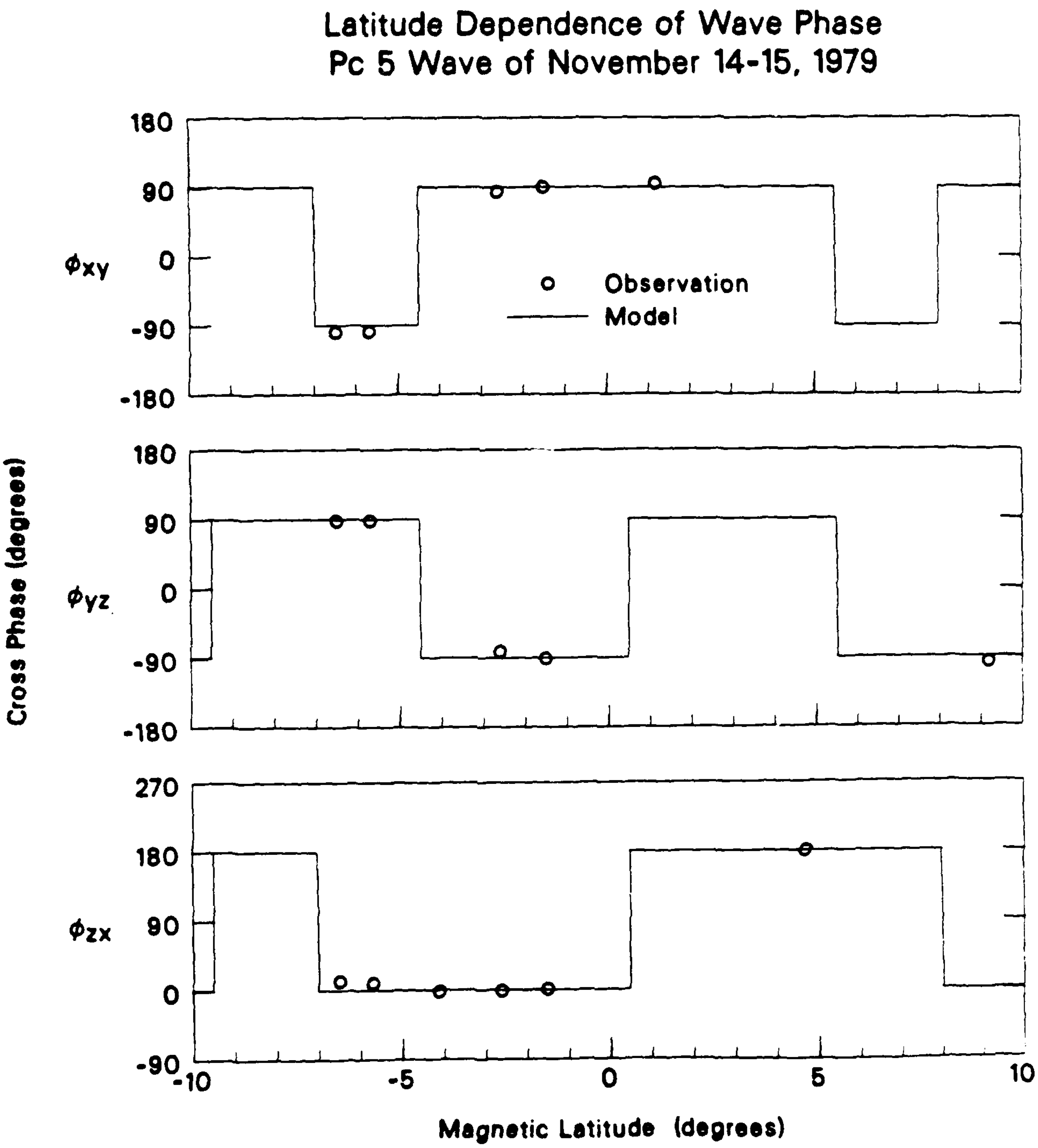

Figure 6. Intercomponent Cross Phase of the Wave Given from Observation (circles) and a Model (lines)

-1° and 4°.

We can argue that only b_y has a clear indication of a node within the latitude range covered by the SCATHA data. Figure 7 illustrates the latitude dependence of the normalized amplitude of the transverse magnetic field components and the phase lag between them. Note that we used only the transverse components for the normalization in order to emphasize the difference between the x and y components. That is, we have defined

$$\hat{b}^{*}_{\alpha} \equiv \left(\frac{\langle b^2_\alpha \rangle}{\langle b^2_x \rangle + \langle b^2_y \rangle}\right)^{1/2}, \quad \alpha = x \text{ or } y.$$

Also, we used the mean variance $\langle b^2_x \rangle$ or $\langle b^2_y \rangle$ calculated on a cycle-by-cycle basis as an indicator of the amplitude, where the wave cycle was defined as the interval between two successive peaks of b_z. This method allows us to determine the latitude structure of the wave in a fine scale and also to evaluate the degree of data scattering at a given magnetic latitude. The middle panel indicates that b_y has a relative minimum at $\lambda \sim 4^\circ$, and the lower panel indicates that a change in relative phase occurred somewhere between $\lambda = -4.2^\circ$ and $\lambda = -3.3^\circ$. These observations can be taken as resulting from a node of b_y located near -4°. The value of ϕ_{xy} is constant between $\lambda = -6.6^\circ$ and $\lambda = -4.2^\circ$, and also between $\lambda = -3.3^\circ$ and $\lambda = -1.2^\circ$, from which we conclude that there is no node for b_x or b_y in these latitude ranges. This conclusion is further confirmed when we compare the amplitude

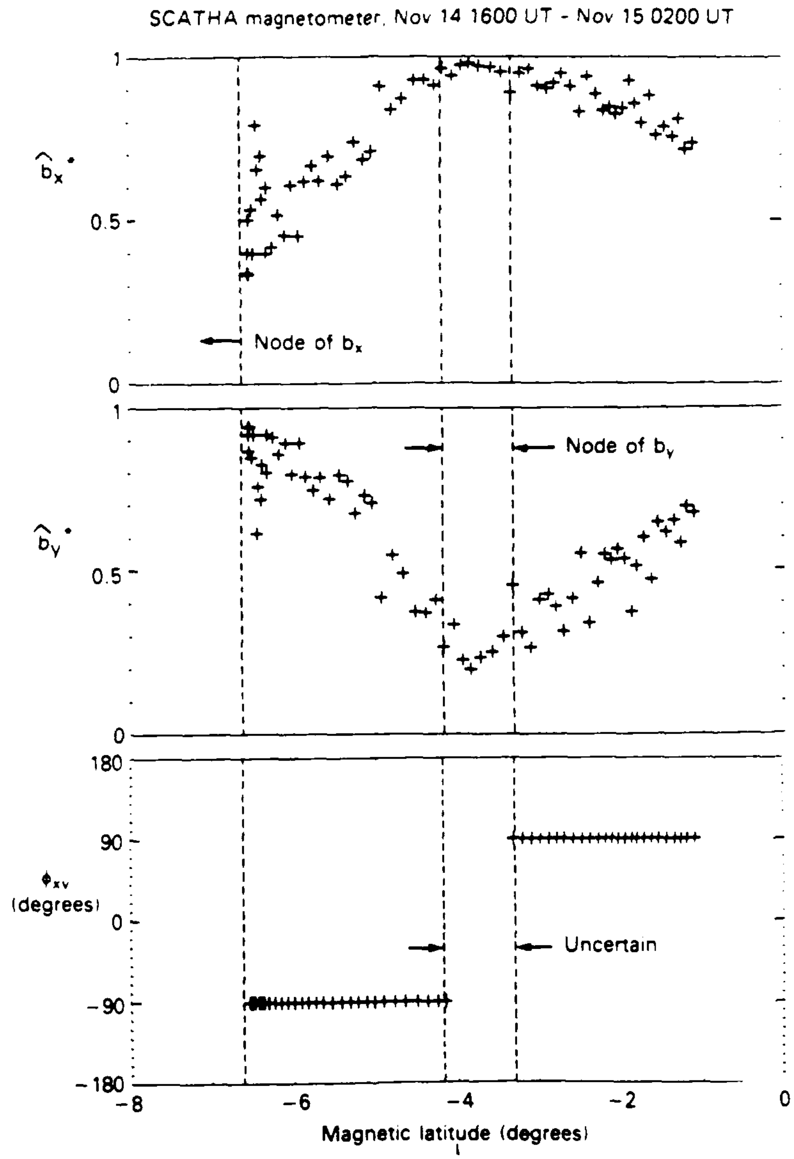

Figure 7. Cycle-by-Cycle Amplitude and Phase of the Transverse Magnetic Field Components. The vertical lines indicate a possible latitudinal range of the nodes of a standing wave. The relative phase ϕ_{xy} was determined by eyeball examination of the time plots of b_x and b_y. Whenever b_x (b_y) led b_y (b_x) by a phase difference smaller than 180°, the value of ϕ_{xy} was set to 90° (-90°).

plots between the two components. The minimum value of $\hat{b}_y^*$, corresponding to a b_y node, is ~0.2, not exactly 0. This can be regarded as the result of noise added to the wave. Assuming that the noise has the same amplitude for b_x, we would expect that $\hat{b}_x^*$ would also reach ~0.2 at its node. All the data points for the component shown in the upper panel, however, are greater than 0.3; therefore we conclude that no node of b_x exists between $\lambda = -6.6^\circ$ and $\lambda = -1.2^\circ$.

From an inspection of the GOES 2 data, on the other hand, we can conclude that a node of b_x is located near the GOES 2 latitude of 9.2°. In Figure 2, the overall amplitude of the x component at GOES 2 is almost null. As an exception, the three wave cycles between 1825 and 1845 UT indicate a small but finite amplitude of b_x, and during this period b_x leads b_y by ~90°, which is the same as the observation near the equator made by SCATHA or GEOS 2. This phase relation can be explained by assuming that a node was located between the equator and GOES 2 for both b_x and b_y, since ϕ_{xy} changes by 180° each time a node is crossed. However, we maintain the view that b_x and b_y have different node latitudes, as was the case with the SCATHA observation. An inspection of the ratio between b_x and b_y in the upper two panels of Figure 3 leads to the conclusion that b_y has a node near GOES 3 (5°), while b_x has a node near GOES 2 (9°).

3.2 Harmonics

An interesting wave form is observed in b_y and b_z. An example is seen in the b_z trace of the lower panel (GEOS 2) of Figure 4. In this case b_z has an amplitude smaller than the transverse components, but we can see that it oscillates at twice the frequency of b_x and b_y. The b_z wave form is not a simple sinusoid: two consecutive peaks do not have the same height except near 1050UT.

Coleman [1970], who analyzed ATS 1 magnetic field data, was the first to report on this type of wave form. He called it the "rectified" version of b_x. Kokubun [1985] found the same phenomenon in GOES 2 and GOES 3 data and called it a "harmonic." Kokubun speculated that this phenomenon is localized in magnetic latitude, because the harmonic was more often observed at GOES 3 ($\lambda \sim 5^\circ$) than at GOES 2 ($\lambda \sim 9^\circ$).

Our data set from the four satellites clearly demonstrates that Kokubun's speculation is correct: the harmonic b_z oscillation occurred only at $\lambda \sim 1^\circ$ in our case. The persistence of this phenomenon and its stability in latitudinal localization was confirmed by scanning the data for 0600-2400UT of November 15, the interval following the one analyzed above. Only GEOS 2 ($\lambda \sim 1^\circ$), among the four satellites, observed the harmonic.

A careful inspection of the GOES 3 data in Figure 4 (its expanded version is shown in Figure 8) reveals that a similar wave form occurs at $\lambda \sim 5^\circ$ in b_y. Although the wave form is essentially the same as for b_z, in this case it is not appropriate to call b_y the rectified version of any other components because the peaks occur at epochs when b_x and b_z are close

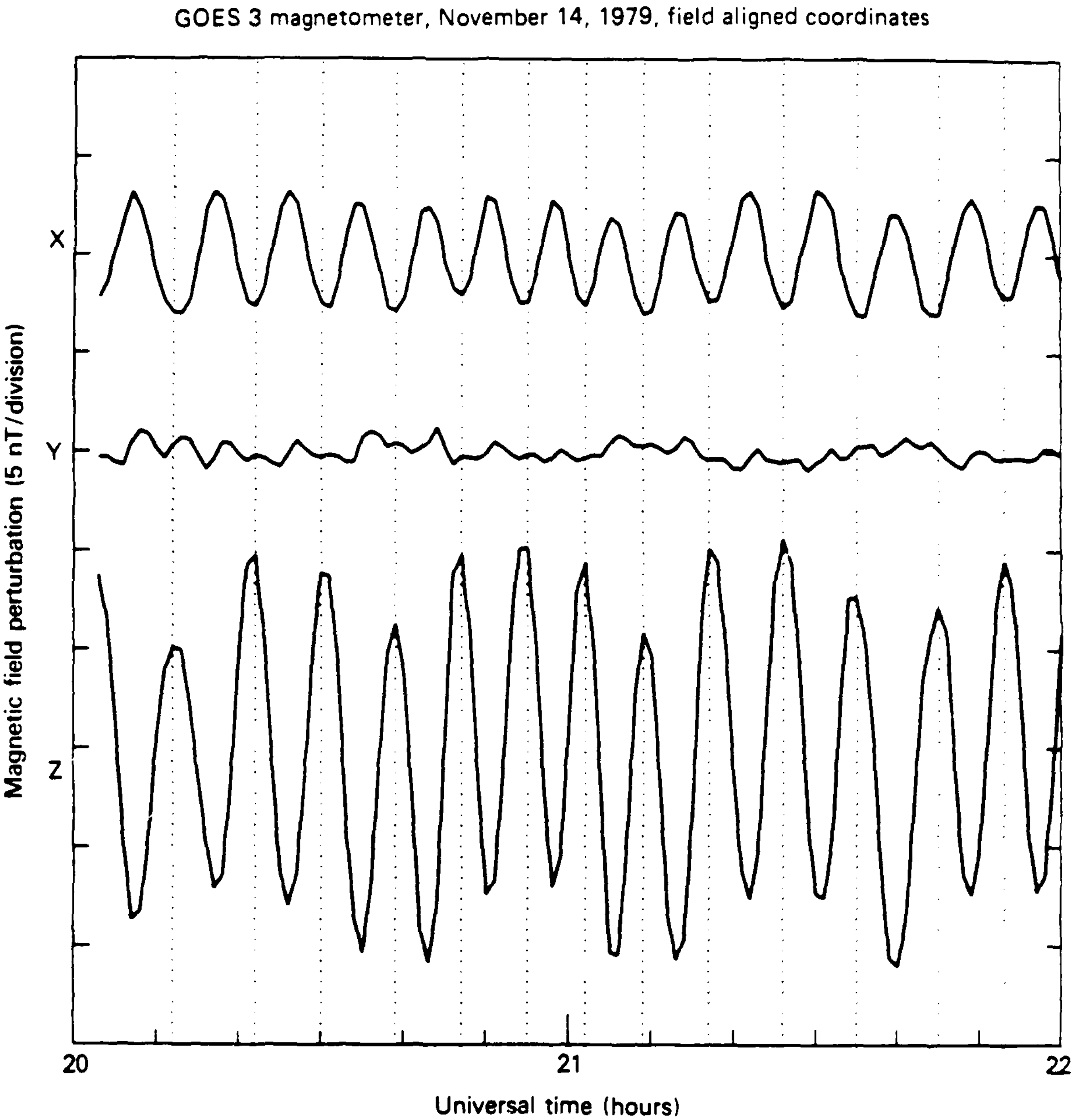

Figure 8. Expanded Version of the GOES 3 Magnetic Field Data Shown in Figure 4. Notice the "harmonic" in the y component.

to zero.

4. Phenomenological Model

A simple phenomenological standing wave model can be constructed to describe the observed latitude dependence of the amplitude and phase of the wave. The model we adopted and show in Figures 5 and 6 has the following form:

$$b_x = \beta_x \cos\{k_z(z-z_o)\} e^{i(k_y y-\omega t)} \quad (1a)$$

$$b_y = i\beta_y \cos\{k_z'(z-z_o)\} e^{i(k_y y-\omega t)} \quad (1b)$$

$$b_z = -\beta_z \sin\{k_z'(z-z_o)\} e^{i(k_y y-\omega t)} \quad (1c)$$

where β_α (α = x, y, or z), k_z, k_z', and ω are real and positive. The phase factor $e^{i(k_y y-\omega t)}$ takes into account the observed azimuthal propagation of the wave. According to Takahashi et al. [1985a], who studied the same wave event, $k_y \sim \frac{-2\pi}{0.6}$ (R_E^{-1}), where the minus sign means westward propagation. The relative phase among the components at any latitude (i.e., z coordinate) can be derived by taking the real part of (1a)-(1c).

The parameters in (1a)-(1c) are determined by trial and error. A reasonable fit to the data was obtained with $\beta_x:\beta_y:\beta_z = 4:3:8$, $k_z = \frac{2\pi}{3.5}$ (R_E^{-1}), $k_z' = \frac{2\pi}{2.3}$ (R_E^{-1}), and $z_o = 0.085\ R_E$, where z_o accounts for the apparent offset of the wave node from the nominal magnetic equator. The fitting of the model was done using the 2-hour data points. Although the model has nodes for b_x and b_y at latitudes slightly different than those discussed in section 3 using cycle-by-cycle wave analysis, the important fact that the different components can have different node latitudes is well taken into account. In practice, z_o is much smaller than the parallel wavelength, so we can regard that the node (anitnode) of b_z (b_x and b_y) lies at the equator. This means that the wave has an antisymmetric standing wave structure.

Because we are trying to model the wave over the latitudinal range from -7° to 9°, we can use an approximation $z \sim LR_E\lambda$ to relate the magnetic latitude to distance along the field line. We assumed in Figure 5 and Figure 6 that the relative phase and the normalized amplitude are a function of magnetic latitude only. Thus the corresponding wavelength depends on the L value. The values for k_z, k_z', and z_o used above correspond to the geostationary distance L ~ 6.6. We should also emphasize that the model (1a)-(1c) probably applies only to the latitudinal range of $\lambda \sim -10^\circ$ to $\lambda \sim 10^\circ$, in which geostationary satellites stay. At present we have no knowledge how the wave structure might change for $|\lambda| \geq 10^\circ$. However, it is obvious because of the inhomogeneity of the ambient magnetic field, we cannot simply assume that the wave field changes with the same wavelength all the way to the ionosphere.

5. Discussion

The observations presented above and summarized in terms of a simple standing wave model have the following physical implications.

5.1. Short parallel wavelength

We have clearly observed nodes for the transverse components at several degrees off the dipole equator. This means that the parallel wave length is only a few earth radii for the components. We have observed only one node for the compressional component,but this is because of the limited latitude coverage of the satellites. It is very likely that the compressional component also has a parallel wavelength of a few earth radii. Such a short parallel wavelength is not consistent with the model in which a compressional wave (drift-mirror mode) is coupled to the fundamental mode of the guided poloidal wave (shear Alfven mode) as was suggested by Walker et al. [1982]. A fundamental mode has half a wavelength along the geomagnetic field line,which means a wavelength of 30 R_E or so at $L \sim 6.6$. In fact, with the wave frequency of 0.002mHz and the parallel wavelength ($\sim 3\ R_E$) obtained above, any shear Alfven resonance $\omega - k_z V_A = 0$ is not likely, where V_A is the Alfven velocity. From the frequencies of multiharmonic standing Alfven waves, the equatorial plasma mass density during the November 14 event has been estimated to be 25 amu/cm^3 [Takahashi et al., 1985a]. For this density, the Alfven wave must satisfy the dispersion relation $\omega/k_z = V_A = 400$ km/s at geosynchronous orbit. However, from the ω and k_z of our Pc 5 wave, we find $\omega/k_z = 40$ km/s, which is in great disagreement with the dispersion relation.

5.2 Multiple wavelengths

The two transverse components. b_x and b_y, have nodes at different magnetic latitudes. The same phenomenon was observed by the ISEE-1 and -2 spacecraft by Takahashi et al. [1985b]. They explained the observation by invoking a symmetric wave for b_y and an symmetric wave for b_x. With our present observation, we conclude that it is not necessary to assume the symmetric and antisymmetric combination. All the components oscillate in an antisymmetric mode, but the wavelength is component dependent.

Southwood and Kivelson [1986] theoretically demonstrated that a compressional wave and a transverse wave can have different amplitude variations along the field line, provided that the plasma density has a gradient along the field line. Although in their argument a box-model of the magnetosphere and a cold plasma were assumed, the essential ingredient of the theory, the field aligned density gradient, should be generally present in the real magnetosphere; therefore, their theory may apply to our result.

5.3. Polarization

The magnetic field perturbation of the wave has components in the x, y, and z directions. The relative phase among the magnetic field components, as illustrated in Figure 6, is either 0, ±90°, or 180° and switches by 180° as the observing satellites move across the nodes of the wave. Here we demonstrate that these polarization characteristics can be explained in terms of wave propagation in an inhomogeneous medium. What follows is a slight modification to the discussion given by Walker et al. [1982].

In general, the perturbation electric field $\underline{E}$ for a wave having a wave vector $\underline{k}$ satisfies

$$\underline{k}\,(\underline{k}\cdot\underline{E}) - k^2\underline{E} + (\underline{\underline{I}} + \underline{\underline{\epsilon}})\cdot\underline{E} = 0$$

where $\underline{\underline{\epsilon}}$ is the dielectric tensor. Walker et al. [1982] derived the expression of $\underline{\underline{\epsilon}}$ for a wave propagating perpendicular to the gradient of the magnetic field strength in a plasma which is characterized by ion guiding center drift. Using their result, we find that the transverse electric field components E_x and E_y are related as

$$-[(\beta_{\parallel} - \beta_{\perp} - 2)k_z^2 + \frac{2\omega^2}{V_A^2}]E_y + ik_yK(\beta_{\parallel} + \beta_{\perp})E_x = 0. \qquad (2)$$

We have neglected electron pressure, which is small in the storm time ring current region. The parameter K, which is real and positive, is equivalent to the inverse gradient scale length of the magnetic field intensity. Since a local approximation has been made, equation (2) is valid for the case $|k_y| >> K$, ℓ_x^{-1}, where ℓ_x is the radial scale length of the wave field. For a wave field which varies as $\exp[i(k_y y + k_z z - \omega t)]$, we obtain from Faraday's law

$$-k_z E_y = \frac{\omega}{c} b_x \tag{3a}$$

$$k_z E_x = \frac{\omega}{c} b_y \tag{3b}$$

$$-k_y E_x = \frac{\omega}{c} b_z \tag{3c}$$

where $\partial E_y/\partial x = 0$ is used in the spirit of local approximation. Also we assumed $E_z = 0$.

In the manner described by Walker et al. [1982] we can construct a standing wave by the superposition of two propagating waves. Unlike Walker et al. [1982], who assumed a symmetric mode, we shall assume an antisymmetric mode for the standing wave. In this model, we take that the radial magnetic field perturbation consists of the following two wave components

$$b_x^+ = \frac{1}{2} A e^{i(k_y y + k_z z - \omega t)}$$

and

$$b_x^- = \frac{1}{2} Ae^{i(k_y y - k_z z - \omega t)}$$

where A is a constant representing the amplitude of the waves. Omitting the common phase factor $e^{i(k_y y - \omega t)}$, the perturbations in other field components corresponding to the above waves can be obtained from (2) and (3a)-(3b) as

$$b_y^{\pm} = - \frac{i\alpha k_z^2}{k_y K} b_x^{\pm} \tag{4a}$$

$$b_z^{\pm} = \pm \frac{i\alpha k_z}{K} b_x^{\pm} \tag{4b}$$

where we have defined

$$\alpha \equiv - \frac{-[(\beta_{\parallel} - \beta_{\perp} - 2) + \dfrac{2\omega^2}{V_A^2 k_z^2}]}{(\beta_{\parallel} + \beta_{\perp})} .$$

Then, the standing wave structure for each component becomes

$$b_x = b_x^+ + b_x^- = A\cos(k_z z) \tag{5a}$$

$$b_y = b_y^+ + b_y^- = -\frac{i\alpha k_z^2}{k_y K} A\cos(k_z z) \tag{5b}$$

$$b_z = b_z^+ + b_z^- = -\frac{\alpha k_z}{K} A\sin(k_z z) \ . \tag{5c}$$

From the discussion presented above, $k_z^2 \gg \frac{\omega^2}{V_A^2}$ holds for our observation, and from SCATHA plasma experiment, we have $\beta_\perp$ = 0.23-0.30 and $\beta_\parallel$ = 0.16-0.21. Those taken into account, we find $\alpha > 0$. Then, taking $k_y < 0$ to be consistent with the observed westward propagation, we find that (5a)-(5c) have the same form as (1a)-(1c) except for the different parallel wavelengths for different components and a small shift of the node from the equator. Thus if we ignore these minor points, the observed phase relations among the components can be explained by the technique of Walker et al. [1982].

Walker et al. associated b_x with a shear Alfven wave and b_y and b_z with a drift-mirror wave. They argued that the drift-mirror wave propagates at the guiding center drift velocity of ions instead of the diamagnetic drift velocity as was originally discussed by Hasegawa [1969]. This argument has some observational support: our wave propagated westward at a velocity of ~10 km/s, the guiding center drift velocity expected for ring current ions with energy of ~10 keV. However, the drift-mirror instability condition was not satisfied, at least at the SCATHA location. Walker et al. further argued that the wave is excited when the coupling condition $\omega = k_y V_d = k_z V_A$ between the drift-mirror wave and the Alfven wave is satisfied, where V_d is the guiding center drift velocity of ions. As discussed above, this prediction does not match our observation either, as discussed above. It seems that Walker et al.'s theory has a limited success here.

5.4. Antisymmetric standing wave structure

Our Pc 5 wave clearly had an antisymmetric standing wave structure. At present we do not know why this is the case. Drift mirror instability of Hasegawa [1969] or Walker et al. [1982] does not have a mechanism to excite an antisymmetric wave preferentially, because the slab geometry which they assumed does not take into account the presence of plasma and field inhomogeneity in the direction of the ambient magnetic field or the presence of bouncing particles.

In view of bounce-drift resonance excitation of ULF waves in the earth's dipole field [Southwood, 1976], there is an intimate relation between the field-aligned structure of the wave and the type of resonance. On one hand there is drift resonance $\omega - m\omega_d = 0$, which could lead to generation of symmetric standing waves. Here, m is the azimuthal wave number, and ω_d is the drift frequency of a given ion species. This preference for symmetric waves does not allow us to apply the resonance to our observation, although the wave angular velocity $\omega/m = \omega_d$ predicted by the resonance condition could explain why the wave propagates westward at a velocity (~10 km/s) comparable to the guiding center drift velocity of the ring current ions (~10 keV).

On the other hand, the drift-bounce resonance $\omega - m\omega_d = \pm\omega_b$ is related to generation of antisymmetric waves, where ω_b is the bounce frequency. Because of the added term on the right-hand side of the equation, this resonance condition does not always imply westward propagation (i.e., $\omega/m < 0$). However, we could estimate the energy of protons which is consistent with the observed values of $\omega \sim 2$ mHz and $m \sim -60$ [Takahashi et al., 1985a]. Using the formula of Hamlin et al. [1961] for particles mirroring near the equator, we find that protons of ~0.3 keV or ~400 keV can satisfy the resonance condition $\omega - m\omega_d = \pm\omega_b$. Such energy is outside the typical energy range of ring current protons; hence this resonance mechanism condradicts the view that the ultimate energy source for storm time Pc 5 waves is the ring current ions.

5.5 Harmonics

If a bounded plasma has an MHD eigenmode (ω, $\underline{k}$), its harmonic (2ω, $2\underline{k}$) is also an eigenmode. So, a simple way to explain the observed harmonic is to assume a small-amplitude wave with 2ω and $2\underline{k}$. For example, we may have

$$b_y = i\delta_y \sin 2k_z'(z-z_o)\ e^{2i(k_y y-\omega t)} \quad (6a)$$

$$b_z = -\delta_z \cos 2k_z'(z-z_o)\ e^{2i(k_y y-\omega t)} \quad (6b)$$

superposed on the wave described by (1a)-(1c), where $\delta_y \ll \beta_y$ and $\delta_z \ll \beta_z$. We assumed that each component of (6a) and (6b) has the symmetry opposite to that of its counterpart in (1b) and (1c). This is necessary in order to have a finite-amplitude harmonic at the nodes of the "fundamental" wave described by (1a)-(1c), but we cannot offer an explanation why this is so.

Such a description is highly phenomenological, and there could be other ways than (6a) and (6b) to describe the observed harmonics [Higuchi et al., 1986; Takahashi et al., 1987]. The questions of whether the harmonic is a general property of storm time Pc 5 waves and whether it has any fundamental importance to the wave excitation mechanism need to be answered by further observational and theoretical work.

6. Conclusion

In conclusion we have presented convincing evidence that the Pc 5 wave of November 14-15, 1979, had an antisymmetric standing wave structure with a parallel wavelength of a few earth radii. Although the event was unusual in that it lasted for such a long period as ~50 hours, we speculate that the structure could be common to other storm time Pc 5 waves.

Previously proposed theories on storm time Pc 5 waves did not take into account an antisymmetric standing wave structure or a short wave length along the ambient field lines. Naturally they fail to give an explanation for our present observation. A new theoretical development seems to be required for the excitation mechanism of storm time Pc 5 waves.

References

Allan, W., E. M. Poulter, and E. Nielsen, STARE observation of a Pc 5 pulsation with large azimuthal wave number, J. Geophys. Res., 87, 6163, 1982.

Brown, W. L., L. J. Cahill, Jr., L. R. Davis, C. E. McIlwain, and C. S. Roberts, Acceleration of trapped particles during a magnetic storm on April 18, 1965, J. Geophys. Res., 73, 153, 1968.

Coleman, P. J., Jr., Geomagnetic storms at ATS 1, in Intercorrelated Satellite Obervations Related to Solar Events, edited by V. Manno and D. E. Page, pp. 251-279, D. Reidel, Dordrecht-Holland, 1970.

Fennell, J. F., Description of P78-2 (SCATHA) satellite and experiments, in IMS Source Book, edited by C. T. Russell and D. J. Southwood, pp. 65-81, American Geophysical Union, Washington, D. C., 1982.

Grubb, R. N., The SMS/GOES space environment monitor subsystem, NOAA Tech. memo. SEL-42, Space Environ. Lab., Natl. Oceanic and Atmos. Admin., Boulder, Colo., 1975.

Hamlin, D. A., R. Karplus, R. C. Vik, and K. M. Watson, Mirror and azimuthal drift frequencies for geomagnetically trapped particles, J Geophys. Res., 66, 1, 1961.

Hasegawa, A., Drift mirror instability in the magnetosphere, Phys. Fluids, 12, 2642, 1969.

Higbie, P. R., D. N. Baker, R. D. Zwickl, R. D. Belian, J. R. Asbridge, J. F. Fennell, B. Wilken, and C. W. Arthur, The global Pc 5 event of November 14-15, 1979, J. Geophys. Res., 87, 2337, 1982.

Higuchi, T., S. Kokubun, and S. Ohtani, Harmonic structure of compressional Pc 5 pulsations at synchronous orbit, Geophys. Res. Lett., 13, 1101, 1986.

Kokubun, S., Statistical characteristics of Pc 5 waves at geostationary orbit, J. Geomag. Geoelect., 37, 759, 1985.

Knott, K., The availability of GEOS data for IMS research, in IMS Source Book, edited by C. T. Russell and D. J. Southwood, pp. 43-52, American Geophysical Union, Washington D.C., 1982.

Lin, C. S., and G. K. Parks, The coupling of Alfven and compressional waves, J. Geophys. Res., 83, 2628, 1978.

Lin, C. S., and J. N. Barfield, Azimuthal propagation of storm time Pc 5 waves observed simultaneously by geostationary satellites GOES 2 and GOES 3, J. Geophys. Res., 90, 11075, 1985.

Nagano, H., and T. Araki, Long-duration Pc 5 pulsations observed by geostationary satellites, Geophys. Res. Lett., 10, 908, 1983.

Pokhotelov, O. A., V. A. Pilipenko, and E. Amata, Drift anisotropy instability of a finite-β magnetospheric plasma, Planet. Space Sci., 33, 1229, 1985.

Southwood, D. J., A general approach to low-frequency instability in the ring current plasma, J. Geophys. Res., 81, 3340, 1976.

Southwood, D. J., and M. G. Kivelson, The effect of parallel inhomogeneity on magnetospheric hydromagnetic wave coupling, J. Geophys. Res., 91, 6871, 1986.

Takahashi, K., and P. R. Higbie, Antisymmetric standing wave structure associated with the compressional Pc 5 pulsation of November 14, 1979, J. Geophys. Res., 91, 11163, 1986.

Takahashi, K., P. R. Higbie, and D. N. Baker, Azimuthal propagation and frequency characteristic of compressional Pc 5 waves observed at geostationary orbit, J. Geophys. Res., 90, 1473, 1985a.

Takahashi., K., C. T. Russell, and R. R. Anderson, ISEE 1 and 2 observation of the spatial structure of a compressional Pc 5 wave, Geophys. Res. Lett., 12, 613, 1985b.

Takahashi, K., L. J. Zanetti, and T. A. Potemra, A model for the harmonic of compressional Pc 5 waves, Geophys. Res. Lett., in press, 1987.

Walker, A. D. M., R. A. Greenwald, A. Korth, and G. Kremser, STARE and GEOS2 observations of a storm time Pc 5 ULF pulsation, J. Geophys. Res., 87, 9135, 1982.

Walker, A. D. M., H. Junginger, and O. H. Bauer, GEOS 2 plasma drift velocity measurements associated with a storm time Pc 5 pulsation, Geophys. Res. Lett., 10, 757, 1983.

LABORATORY OPERATIONS

The Aerospace Corporation functions as an "architect-engineer" for national security projects, specializing in advanced military space systems. Providing research support, the corporation's Laboratory Operations conducts experimental and theoretical investigations that focus on the application of scientific and technical advances to such systems. Vital to the success of these investigations is the technical staff's wide-ranging expertise and its ability to stay current with new developments. This expertise is enhanced by a research program aimed at dealing with the many problems associated with rapidly evolving space systems. Contributing their capabilities to the research effort are these individual laboratories:

Aerophysics Laboratory: Launch vehicle and reentry fluid mechanics, heat transfer and flight dynamics; chemical and electric propulsion, propellant chemistry, chemical dynamics, environmental chemistry, trace detection; spacecraft structural mechanics, contamination, thermal and structural control; high temperature thermomechanics, gas kinetics and radiation; cw and pulsed chemical and excimer laser development including chemical kinetics, spectroscopy, optical resonators, beam control, atmospheric propagation, laser effects and countermeasures.

Chemistry and Physics Laboratory: Atmospheric chemical reactions, atmospheric optics, light scattering, state-specific chemical reactions and radiative signatures of missile plumes, sensor out-of-field-of-view rejection, applied laser spectroscopy, laser chemistry, laser optoelectronics, solar cell physics, battery electrochemistry, space vacuum and radiation effects on materials, lubrication and surface phenomena, thermionic emission, photosensitive materials and detectors, atomic frequency standards, and environmental chemistry.

Computer Science Laboratory: Program verification, program translation, performance-sensitive system design, distributed architectures for spaceborne computers, fault-tolerant computer systems, artificial intelligence, microelectronics applications, communication protocols, and computer security.

Electronics Research Laboratory: Microelectronics, solid-state device physics, compound semiconductors, radiation hardening; electro-optics, quantum electronics, solid-state lasers, optical propagation and communications; microwave semiconductor devices, microwave/millimeter wave measurements, diagnostics and radiometry, microwave/millimeter wave thermionic devices; atomic time and frequency standards; antennas, rf systems, electromagnetic propagation phenomena, space communication systems.

Materials Sciences Laboratory: Development of new materials: metals, alloys, ceramics, polymers and their composites, and new forms of carbon; nondestructive evaluation, component failure analysis and reliability; fracture mechanics and stress corrosion; analysis and evaluation of materials at cryogenic and elevated temperatures as well as in space and enemy-induced environments.

Space Sciences Laboratory: Magnetospheric, auroral and cosmic ray physics, wave-particle interactions, magnetospheric plasma waves; atmospheric and ionospheric physics, density and composition of the upper atmosphere, remote sensing using atmospheric radiation; solar physics, infrared astronomy, infrared signature analysis; effects of solar activity, magnetic storms and nuclear explosions on the earth's atmosphere, ionosphere and magnetosphere; effects of electromagnetic and particulate radiations on space systems; space instrumentation.

END
DATE
FILMED
DTIC
JULY 88